Anodically bonded submicron microfluidic chambers

S. Dimov,[1] R. G. Bennett,[2] A. Córcoles,[2,a)] L. V. Levitin,[2] B. Ilic,[1] S. S. Verbridge,[1] J. Saunders,[2] A. Casey,[2] and J. M. Parpia[2]
[1]*Department of Physics, Cornell University, Ithaca, New York 14853, USA*
[2]*Department of Physics, Royal Holloway University of London, Egham, TW20 0EX Surrey, United Kingdom*

(Received 3 November 2009; accepted 20 December 2009; published online 29 January 2010)

We demonstrate the use of anodic bonding to fabricate cells with characteristic size as large as 7×10 mm^2, with height of ≈640 nm, and without any internal support structure. The cells were fabricated from Hoya SD-2 glass and silicon wafers, each with 3 mm thickness to maintain dimensional stability under internal pressure. Bonding was carried out at 350 °C and 450 V with an electrode structure that excluded the electric field from the open region. We detail fabrication and characterization steps and also discuss the design of the fill line for access to the cavity. © *2010 American Institute of Physics.* [doi:10.1063/1.3291107]

I. INTRODUCTION

Motivated by recent theoretical work,[1–3] there are compelling reasons to initiate investigations on high-aspect-ratio confined superfluid ^{3}He. The characteristic size requirements for the height of the cell is determined by the so-called "zero temperature coherence length," $\xi_0 = \hbar v_F/(2\pi k_B T_c)$, where v_F is the Fermi velocity, k_B is Boltzmann's constant, and T_c is the superfluid transition temperature,[4] while the required area of the structure is determined by the sensitivity of the technique used to assay the helium. The two experiments that have been assembled to date are a 10×7 mm^2 rectangular cavity and a 10 mm outer diameter × 4 mm inner diameter circular cavity, each of 640 nm height. The zero temperature coherence length can be tuned by varying the pressure from ≈77 nm at 0 bar to ≈39 nm at 6 bar, allowing the relevant parameter (cell height/ξ_0) to be tuned by a factor of 2 over a relatively narrow pressure range.

There are also additional requirements for such experiments. There is evidence that the quality of the surface, including details of the surface roughness and correlations, has to be well established since it affects the flow properties of the helium[5–7] through the surface scattering of the quasiparticle excitations. Theoretical work[1–3,8] proposes that an outcome of the confinement is a competition between superfluid phases of nearly equivalent free energy. Of particular interest is the prediction of a region of the phase diagram where the translational symmetry is spontaneously broken in the form of a striped phase.[3] This motivates a design which presents the helium with a featureless slab geometry.

Faced with these requirements, a decision to move away from the use of $Si-SiO_2$ bonding as described by Rhee *et al.*[9] was taken. This was based on anecdotal information about the strength of the $Si-SiO_2$ bond and the requirement to avoid numerous supporting posts. Instead we elected to use conventional anodically bonded cells[10–12] with Hoya SD-2 glass[13] (instead of borofloat) because SD-2 has a thermal expansion coefficient that is well matched to that of silicon over the temperature range above room temperature where the bonding takes place. Since the experiment would call for the operation of the cell at pressures from saturated vapor pressure up to several bar, we built the cell from 3 mm thick silicon and Hoya glass. The thickness of the silicon and glass/cell materials was dictated by making an estimate of the maximum deflection of a rectangular plate fixed around all its edges under a load uniformly distributed over its surface given by[14]

$$d = \frac{0.0284W}{Et^3\left(\frac{L}{l^3} + \frac{1.05612l^2}{L^4}\right)}. \quad (1)$$

Here, W is the load in newton, E is the modulus of elasticity, t is the thickness of the plate, L is the length of the plate, and l is the width of the plate. At a pressure of 6 bar in the cell, $W=42$ N; for silicon, $E=170$ GPa;[15] for the glass, $E=86$ GPa,[13] $L=10$ mm, and $l=7$ mm, resulting in a total maximum deflection of 23 nm, ≈4% of the cavity height. However, the values used above for the elastic moduli of the silicon and glass are both room temperature values, so there is likely to be less deflection at low temperatures when E should be greater.

The silicon and glass surfaces were scanned by atomic force microscope (AFM) probes in an attempt to quantify the surface roughness. Once the bonding was accomplished, we carried out interferometric measurements on the cell height using visible light. In this paper we describe the fabrication details, surface characterization, and interferometric measurements on the cell height as well as the details of the assembly for helium use. Preliminary normal state measurements of the mass coupled to a torsion pendulum have been reported elsewhere.[7] NMR signals[16,17] have been observed from such ^{3}He samples despite the low filling factor using a spectrometer based on a two-stage dc superconducting quantum interference device amplifier.[18]

a)Present address: Department of Physics, University of Cambridge, Cambridge CB3 0HE, United Kingdom.

II. CELL FABRICATION

A. Wafer patterning

The starting material was a ⟨100⟩ orientation single crystal 100 mm diameter wafer. For a finished cell cavity depth of 640 nm, we carried out the following steps.

(1) Deposit 4 μm of SiO_2 using plasma-enhanced chemical-vapor deposition (PECVD) (providing there is no thermal oxide on the wafer).
(2) Prepare a mask with the desired pattern.
(3) Deposit photoresist and pattern on the entire wafer. Develop the photoresist.
(4) Remove the oxide from the patterned surfaces. Strip away remaining photoresist.
(5) Thermal oxidation of the wafer. This consumes the silicon in the patterned region much faster than the silicon under the PECVD oxide. There are tables[19] that yield the diffusion rate and rate of growth of the oxide layer under bare and oxidized silicon.
(6) Holes for access of the helium into the cavity are made using an ultrasonic drill. A key feature is the use of a ≈2 mm thick layer of supporting Crystalbond[20] so that the only hard material that the ultrasonic drill is in contact with is the silicon. The wafer is then diced to yield cavities, and the oxide is dissolved away.
(7) The silicon is now ready for anodic bonding to the glass. The glass "lid" is diced (oversize) in preparation for bonding.
(8) A silver layer (for thermalization) is evaporated on the exterior of the cavity. The hole for the fill line is covered with a brass plug to prevent contamination of the interior.
(9) The fill line is glued in as the last step.

A schematic version of the essential steps is shown in Fig. 1.

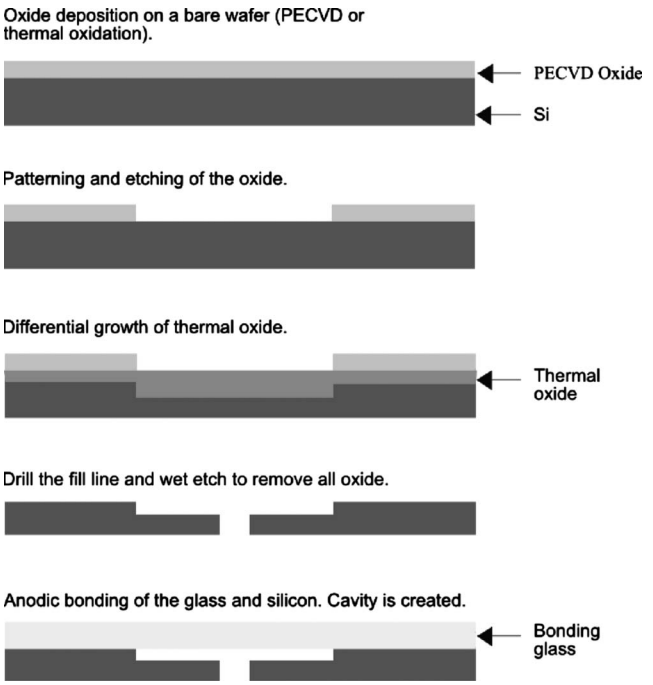

FIG. 1. The sequence of essential steps in the patterning of the silicon that comprises one side of the ^{3}He cell and its final form when bonded to the glass.

B. Cavity designs

At the outset we had to establish the limitations of the fabrication of large area cavities. We elected to maintain a 3 mm wide bonding area on the periphery of the NMR cavities and 3.5 mm wide for the torsion pendulum cavities. The two experimental probes we have focused on impose different demands on the geometry of the cavity. For torsional oscillator measurements, a cylindrical cavity is required to maintain symmetry about the axis of oscillation and minimize the fluid inertia coupled to the structure by forces other than via the shear viscosity.[7] For NMR measurements on ^{3}He, our design called for a rectangular geometry with a fill line located away from the main cavity. This was desirable in order that the helium contained in the fill line (potentially far greater in volume than the helium in the cavity) could be shielded from the magnetic field or located in a field that is different from that on the main cavity. The difference in magnetic field strength allows us to distinguish the ^{3}He NMR signal arising from the "bulk" and from the cavity regions.

The first design's goal was to establish the largest dimension structure that could be fabricated without encountering collapse of the cavity walls during bonding. There have already been extensive investigations of the collapse of microchannels during anodic bonding.[12] That work established a critical width, a_c, that is related to the effective elastic modulus, E_e, the effective voltage V_e=applied voltage/2, cavity height, d, and ϵ_a, the permittivity of air. The expression for a_c is given by

$$a_c = \frac{E_e d^3}{\epsilon_a V_e^2}. \tag{2}$$

We used the value for E_e=51 GPa from Shih *et al.*[12] because material properties (at elevated temperatures) for the Hoya SD-2 are not as well known as those for borosilicate glass. At an applied voltage of 750 V (more than sufficient to ensure bonding), we expected the critical width a_c=10 mm. We found that cavities larger than 3 mm width collapse for even the lowest feasible voltage (400 V). Thus we had to modify the process if cell construction were to proceed.

Since the collapse is presumably induced by the electric field, our solution was to exclude the electric field from regions where bonding was not to take place. This was done by patterning a brass electrode (located above the glass in the glass-silicon sandwich) with a simplified version of the pattern used to define cavities. A schematic of the test electrode and bonded 100 mm wafer showing the collapse of cavities where the electric field was not excluded, as well as the survival of cavities where the electric field was excluded, is shown in Fig. 2.

Based on these results we elected to limit our designs to a rectangular cavity with a 7 mm width × 10 mm length or a 10 mm diameter circular cavity. To further improve our yield, we decided on a design of the circular cavities that includes a central support bonded region of 4 mm diameter. This region should not significantly affect measurements of

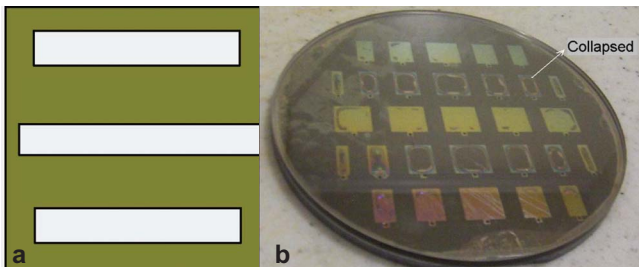

FIG. 2. (Color online) (a) Schematic of electrode that excludes electric field from top, center, and bottom rows. The white areas designate regions where there is no applied electric field. (b) Image of bonded 4 in. wafers showing five rows of cavities. The uniformly collapsed cavities occur in rows where electric field was not excluded, namely, the second and fourth rows from the top. Bonding still occurs in the regions between the various cavities in the top, middle, and bottom rows even in the absence of an applied electric field.

superfluid fraction since the inertial contribution of helium in the oscillator is weighted as r^4. The computer aided design (CAD) layout for the torsional oscillator cavities is shown in Fig. 3.

After these trials, a 4 in. diameter wafer, oxidized as described earlier, was patterned with a series of cavities of identical width and length (or diameter) and fabricated. Holes for the file line were made in the silicon (see next section), following which the silicon was diced into the final size using a water-cooled diamond saw. The Hoya SD-2 glass was also diced into similarly patterned pieces; however a 2 mm excess length or width of glass was left to aid in the final assembly. This excess material was removed using a circular diamond saw once the pieces were anodically bonded.

The anodic bonding on the actual cavities was carried out (postcleaning; see Sec. II D) by applying a force of 70 N across the surface of a 100 mm wafer. When we bonded a single cavity, an area equivalent to the 100 mm wafer was made up with scraps of glass and silicon to maintain the same bonding pressure. The bonding conditions were maintained at 450 V and 350 °C. However before the bonding could be done, the hole for the fill line had to be fabricated and the silicon cleaned.

C. Holes for fill line

Early in the design process, we tested the survival of junctions between silicon (or the Hoya glass) and a silver fill

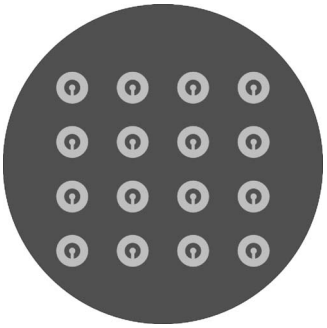

FIG. 3. CAD of the pattern for torsional oscillator cavities. The light gray regions are where the oxide will be grown and removed, thus defining the space where helium will reside.

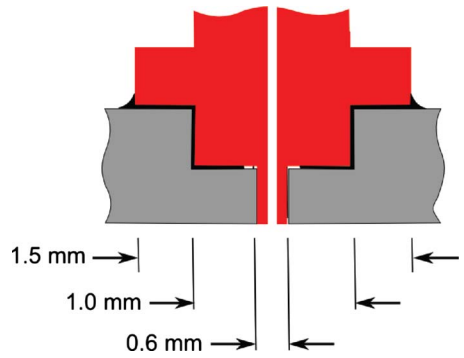

FIG. 4. (Color online) Schematic of the cross section of the hole drilled in the silicon showing detail of the coin silver fill line and epoxy fillet (not to scale).

line after the joints were subjected to rapid thermal shock between room temperature and liquid nitrogen temperature. The joints between a silver tube and an ultrasonically drilled hole in the material were completed with a thin fillet of Stycast 2850 GT epoxy,[21] chosen because of its small thermal expansion coefficient. We found that the glass-epoxy-silver joints failed due to microscopic cracks in the glass, while the silicon-epoxy-silver joints survived intact. Accordingly we elected to pattern the silicon and locate a hole in the silicon to which the fill line would be fastened.

The hole for the transition of the fill line into the cavity was fabricated with a step profile, with the smaller section on the cavity side. The diameters of the two holes were 0.6 and 1.0 mm. The holes were made in a two step process. First the small hole was ultrasonically drilled through the entire wafer. The wafer had been adhered to a steel plate using Crystalbond glue to a depth of 2 mm, the extra depth ensuring that the ultrasonic drilling process could be stopped before the drill contacted the steel plate. The bonding agent was built up to a thickness that extended to the patterned surface of the wafer. Next, the through hole was used as a guide to drill a second (1.0 mm diameter) concentric hole. The fill line would enter through this larger hole. Holes drilled in this manner were found to be free of chips, especially critical for the exit point of the small hole that was on the cavity side. A small chip of sub mm dimensions could readily have a volume exceeding that of the entire cavity.

For both NMR and torsional oscillator cavities, a stepped profile was machined in a coin silver piece that matched the concentric holes in the silicon. The leading (0.6 mm) portion was machined to as close a precision as possible and dry-fitted into the silicon. The 1.0 mm portion had a 0.05 mm radial clearance for epoxy, and a step to 1.5 mm diameter provided for a "flange" where the epoxy would reside and adhere to the silicon and coin silver transition piece. Stycast epoxy 2850 GT was applied to the silver fill line in a band at the 0.6–1.0 mm transition. Once the tip was inserted into the smaller diameter of the stepped profile, epoxy was automatically prevented from entering into the cavity. The fill line was rotated in the hole to distribute the epoxy and promote full coverage and adhesion. Excess epoxy was wiped off to ensure that thermal contraction forces were minimized, leaving a fillet that extended to no more than 2 mm in diameter. The assembly is illustrated in Fig. 4.

D. Cleaning

Once the cavities were fabricated in the silicon, it was necessary to thoroughly clean them to ensure removal of all residue of the Crystalbond and the remaining protective oxide. Contaminants result in nonuniform anodic bonding and height variations and may eventually compromise the leak-tightedness of the cell. The first step in the cleaning is to remove the Crystalbond. Both the silicon and glass pieces were cleaned in an ultrasonic acetone bath for 20 min. This procedure dissolves the majority of the Crystalbond, but once the pieces are taken out of the bath and the acetone evaporates, a thin layer of contamination can be observed on the surfaces. The second cleaning step (RCA SC-1 clean recipe)[22] removes the residual organic contaminants left after the acetone bath. To prepare the recipe we mix de-ionized water, hydrogen peroxide, and ammonium hydroxide with ratios of $H_2O:H_2O_2:NH_4OH=5:1:1$ and heat the mixture to 80 °C. The silicon and glass pieces are immersed in the hot mixture for 30 min. After the RCA clean, the pieces are rinsed in de-ionized water and blown dry with nitrogen. Since we kept the thermal oxide on the silicon wafer for protection, we needed to remove it before the anodic bonding. Immersion of the silicon pieces in buffered oxide etch 6:1 strips the oxide. The silicon pieces are ready for bonding after they are rinsed in de-ionized water and dried off with nitrogen gas. At all times the cavities were handled by the edges with tweezers (the 3 mm thickness of the glass and silicon was helpful in this respect). The bonding was carried out in a clean room to avoid contamination of the cavities with dust.

III. CELL CHARACTERIZATION

A. Roughness

The surfaces were characterized by scanning samples with a DI 3100 AFM. Prior to data acquisition the samples were immersed for 30 min in acetone and immediately before scanning were swabbed with an isopropanol soaked q-tip. A "tapping" cantilever was used for the scan, and it had a diameter of 10 Å. The highest resolution for the microscope, 512×512 pixels, was chosen for all scans. The size of the area scanned under the probe ranged from 2×2 to 50×50 μm^2. The scanned area was selected away from the edges of the wafer (where the material for cavities would be located) so that any scratches that might occur during handling would be avoided.

Raw data for the topography of a 10×10 μm^2 scan of the polished glass are shown in Fig. 5 as an artificial contrast two-dimensional (2D) rendition. The digitized height profile $z(x,y)=z(\tau m,\tau n)=z_{mn}$ provides statistics of surface topography. Here $m,n=0,1,\ldots,N-1$, $N=512$ is the number of pixels in a raw, and $\tau\approx20$ nm is the scan step size. A histogram of the height distribution function obtained from the scan is shown in Fig. 6.

The histogram was generated with a bin size of 0.02 nm for heights in the range of −5 to +5 nm. From the histogram, we can approximate a probability density $f(z)$

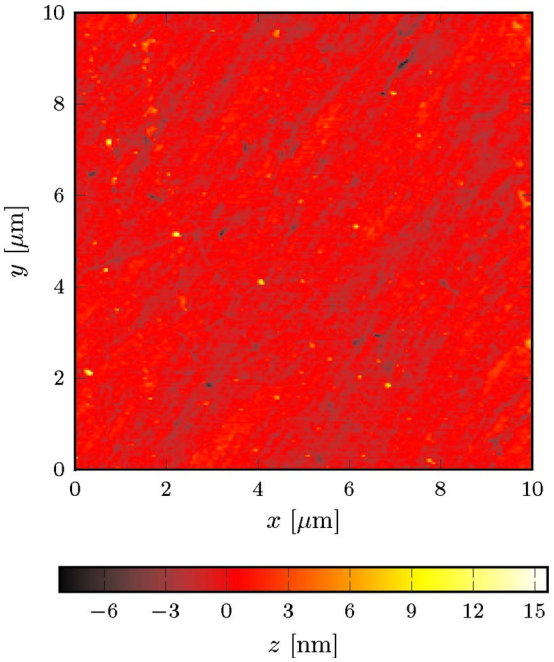

FIG. 5. (Color online) Artificial contrast 2D rendition of a 10×10 μm^2 AFM scan of a Hoya SD-2 glass surface. The digitized $z(x,y)$ profile was used to generate height autocorrelations as well as a histogram of height distribution.

$$f\left(\frac{b_n+b_{n+1}}{2}\right)\approx\frac{N(b_n\leq z<b_{n+1})}{(b_{n+1}-b_n)N_\Sigma}, \tag{3}$$

where b_n are the bin boundaries, N_Σ is the total number of pixels, and $N(b_n\leq z<b_{n+1})$ is the number of pixels in the nth bin. The probability density was fit to a Gaussian

$$f(z)=\frac{1}{\sqrt{2\pi\sigma_G^2}}\exp\left[-\frac{(z-z_0)^2}{2\sigma_G^2}\right], \tag{4}$$

where σ_G is the standard deviation of the height. For the scan shown in Fig. 5 and the height distribution shown in Fig. 6, we obtained $\sigma_G=0.85$ nm. Deviations of the measured heights from the Gaussian distribution increase the actual standard deviation of the height to 1.01 nm.

The surface of the silicon wafer (after patterning as described in Sec. II A) was also scanned using the same AFM apparatus. No comparable topography was mapped on the

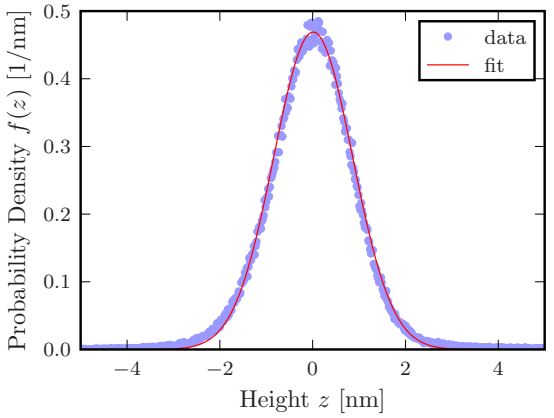

FIG. 6. (Color online) Height distribution data (points) and Gaussian fit (line) to the data. The standard deviation obtained in the fit $\sigma_G=0.85$ nm.

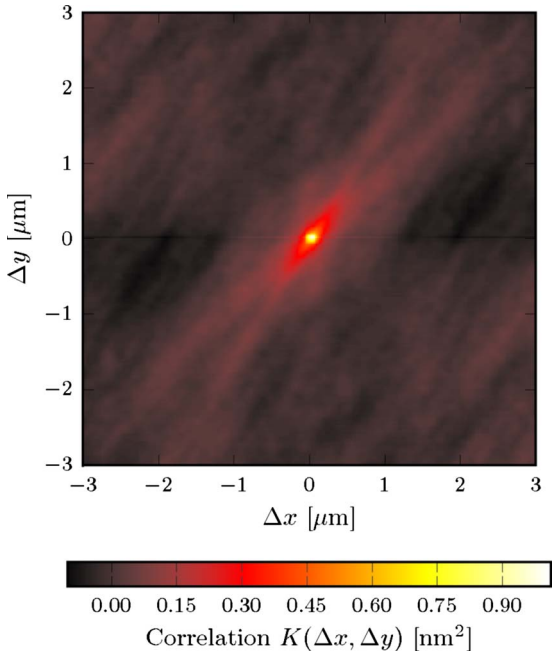

FIG. 7. (Color online) The 2D autocorrelation function of the glass calculated according to the definition [Eq. (6)]. Most relevant are the short-length correlations that contribute to the surface roughness (see Fig. 8).

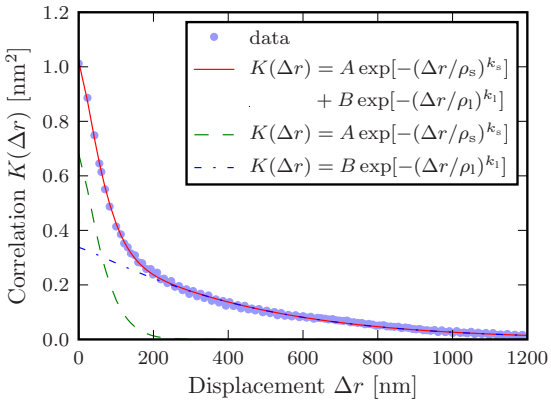

FIG. 8. (Color online) The one-dimensional representation of the autocorrelation function of the glass. The dots (blue) are the calculated autocorrelation function, and the solid line (red) is the double stretched exponential fit. The short- and long-length correlation peaks of the fit are shown separately with a dashed and a dash-dotted line, respectively. The short-range correlation length ρ_s, defined as the distance over which the autocorrelation function drops by a factor of $1/e$, was found to be 73 nm.

surface, so the roughness could not be resolved. We assign an upper bound of 0.2 nm for such a roughness.

B. Correlations

The height distribution function does not reveal correlations between points at different positions. To account for the correlations, we generate a 2D spatial autocorrelation function $K(\Delta x,\Delta y)$. The correlation of two variables is defined as the expected value of the product of those two variables. From this definition, we can write the 2D autocorrelation function as

$$K(\Delta x,\Delta y)=\langle z(x,y)z(x+\Delta x,y+\Delta y)\rangle, \tag{5}$$

which for our discrete finite set of data can be expressed as

$$K(\Delta x,\Delta y)=K(\tau\Delta m,\tau\Delta n)=\langle z_{mn}z_{m+\Delta m,n+\Delta n}\rangle = \frac{\sum_{m=\max(0,-\Delta m)}^{N-\max(0,\Delta m)-1}\ \sum_{n=\max(0,-\Delta n)}^{N-\max(0,\Delta n)-1} z_{mn}z_{m+\Delta m,n+\Delta n}}{(N-|\Delta m|)(N-|\Delta n|)}, \tag{6}$$

where the summation is over m,n such that $0\leqslant m,n,m+\Delta m,n+\Delta n<N$ and τ is the step of the scan. The directly calculated 2D autocorrelation function is shown in Fig. 7.

The autocorrelation function is maximum at the origin, $K(\Delta x,\Delta y)\leqslant K(0,0)$. Furthermore, if one offsets heights so that $\langle z(x,y)\rangle=0$,

$$K(0,0)=\langle z(x,y)^2\rangle=\sigma^2, \tag{7}$$

where σ is the standard deviation of the height distribution (we allow $\sigma\neq\sigma_G$ to account for deviations of the height distribution from the Gaussian form). At large displacements, $\Delta x^2+\Delta y^2\to\infty$, where $z(x,y)$ and $z(x+\Delta x,y+\Delta y)$ are uncorrelated, $K(\Delta x,\Delta y)$ vanishes,

$$K(\Delta x,\Delta y)=\langle z(x,y)\rangle\langle z(x+\Delta x,y+\Delta y)\rangle=0. \tag{8}$$

We can reduce the dimensionality of our data set by assuming the surface to be isotropic. Then, $K(\Delta x,\Delta y)=K(\Delta r)$, with $\Delta r=\sqrt{(\Delta x)^2+(\Delta y)^2}$. From the discrete autocorrelation function, we compute the one-dimensional representation $K(\Delta r)$ by grouping points on the $(\Delta x,\Delta y)$ plane into bins $\tau/2$ wide: $\tau m/2\leqslant\sqrt{\Delta x^2+\Delta y^2}<\tau(n+1)/2, n=0,1,\ldots$, and averaging the autocorrelation function over each bin.

The central peak of the resulting autocorrelation function (Figs. 7 and 8) can be fit by a function that vanishes at infinity. We found that the data could not be fit by a simple exponential form. Therefore we model the autocorrelation function with a stretched exponential form

$$K(\Delta r)=\sigma^2\exp\left[-\left(\frac{\Delta r}{\rho}\right)^k\right], \tag{9}$$

where σ is the standard deviation of the height distribution and ρ is the correlation length defined as the distance over which the autocorrelation function decreases by a factor of e, $K(\rho)/K(0)=1/e$.

We found that a single stretched exponential function could not fit the autocorrelation function over all distances. Therefore, we assumed a combination of correlations with two different characteristic lengths,

$$K(\Delta r)=A\exp\left[-\left(\frac{\Delta r}{\rho_s}\right)^{k_s}\right]+B\exp\left[-\left(\frac{\Delta r}{\rho_l}\right)^{k_l}\right], \tag{10}$$

where the subscripts "s" and "l" refer to the short- and long-range correlations, respectively. The fit, shown in Fig. 8, yields $A=0.68$ nm^2, $k_s=1.36$, $\rho_s=73$ nm, $B=0.34$ nm^2, $k_l=1.13$, and $\rho_l=438$ nm. We find for the peak height of the short-range correlations, $A=0.68$ nm$^2\approx\sigma_G^2$, suggesting that the long-range correlations might be responsible for the deviations from the Gaussian distribution of heights.

Due to the fact that our sample is finite, our definition of the discrete autocorrelation function can only be an estimate of the surface correlations. This particularly affects the long-

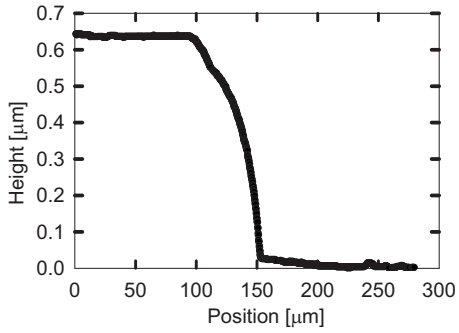

FIG. 9. The profilometer scan of a cavity used for NMR experiments. The recorded value of the scan, 635 nm, is in good agreement with optical measurements.

length scale correlations. It is probable, however, that the short-length scale correlations dominate the transport of ^{3}He, but that is a matter for further investigation.

C. Profilometer scan

Each silicon cavity prior to bonding (but after dicing) was characterized by a scan using a profilometer stylus. The profilometer records the contour as the stylus traverses the step at an edge of the cavity. The profilometer scan of one of our cavities is shown in Fig. 9 and shows a step at the cavity walls with a size of 635 nm.

D. Optical characterization

The cavity height of ≈635 nm is ideal for optical characterization of the size using standard interferometric techniques. We set up several cavities on a standard student-laboratory spectrometer typically used to characterize atomic spectra. The two arms of the spectrometer were modified, one to hold a laser source with an in-line polarizer and the second held a standard diode detector. The spot size used was of the order of 0.2 mm. Two lasers were used: a standard HeNe 665 nm laser diode and a 532 nm Nd:YAG frequency doubled laser to provide checks at different wavelengths. The range of angles scanned was between 20° and 67° angle of incidence from normal. A short-wavelength pass filter was introduced to cut off the 1064 nm component that otherwise overwhelmed the diode sensor when the green laser was used.

A typical data set at a single location consisted of three sets of measurements, one with the red laser with polarizer arranged perpendicular to the reflection plane and two with the green laser with both parallel and perpendicular polarizations. For each measurement configuration, we fit for a constant intensity of laser light, a constant background intensity, and allowed the angle read off from the spectrometer to have a constant (for each wavelength and polarization) error of less than 2°, consistent with the way the laser adapters and detector were fastened to the spectrometer arm. Fits obtained for the perpendicularly polarized 665 nm laser light at a point at 9 o'clock on a circular cavity and for 532 nm laser light for both perpendicular and parallel polarizations are shown in Fig. 10.

We carried out fits using constrained and fitted values of the angles for each of four positions (3, 6, 9, and 12 o'clock)

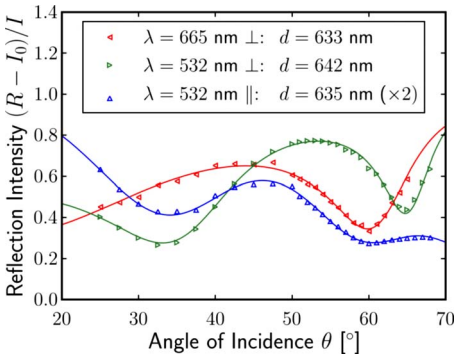

FIG. 10. (Color online) Data obtained on a circular cavity at position 9 o'clock at a point midway between the inner and outer radii. Lines drawn are the best fit through the data, yielding a thickness of 633 nm for the perpendicularly polarized red light, 642 nm for the perpendicularly polarized green light, and 635 nm for the parallel component of the green light. The best fit was obtained with an angle offset of 1.4°.

with one polarization of the red laser and two polarizations of the green laser. The fits are summarized in Fig. 11.

Based on these results we estimate the overall thickness to be 638 nm ± 2 nm. For the individual spots we find 643 ± 3 nm (at 12 o'clock), 636 ± 3 nm (at 9 o'clock), 639 ± 5 nm (at 6 o'clock), and 636 ± 7 nm (at 3 o'clock). These values are consistent with the profilometer scan.

E. Thermal cycling

Because of the use of glass in the cavity, we were mindful of possible virtual heat leaks from the glass into the helium. Experiments at Cornell have observed that imperfectly thermalized glass can have an internal thermal relaxation that results in its cooling to no lower than a few millikelvin,[23] which could result in significant heat leaks via the

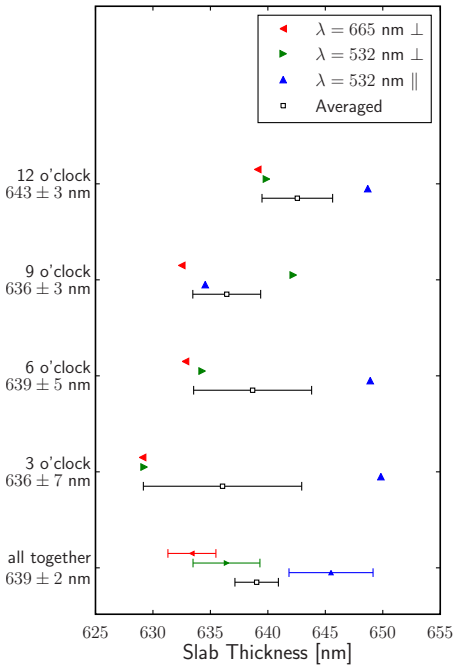

FIG. 11. (Color online) Composite of the fits obtained using two lasers at 4 different locations on a circular cavity. The summaries (with symbols identical to those used in Fig. 10) are shown. Average values (open squares) at each location are also shown.

Kapitza conductance. The silicon wafer was not degenerately doped, and so it too could conceivably have limited thermal conductivity at low temperatures. Accordingly the cavities were coated with a 0.5 μm silver layer that had a residual resistance ratio of 9. In a 640 nm rectangular cavity, superfluid ^{3}He samples were successfully cooled to 0.4 mK, where the NMR frequency shift could be used as an internal thermometer. No problems with thermal equilibration were encountered.

After assembly the cavities were tested at liquid nitrogen temperature on a standard test cryostat. In our original tests for dummy cavities, we thermally cycled the cavities rapidly by immersing them in the vapor and then lowering into liquid over a period of a few minutes without adverse effects. However, once the cavities were completed, we treated them with much greater care.

After characterization, a cavity was cooled in a liquid nitrogen cryostat equipped with a small optical window. The thermal expansion characteristics of Hoya SD-2 are only known down to −40 °C. It is conceivable that the differential contraction of the glass relative to the silicon could result in a distortion of the cavity. By examining the cavity by eye at normal incidence, we were unable to discern any change in the color of the reflected light (a blue green color) upon cooling. We estimate by examining a chart of colors that we can discern a color difference consistent with a variation of ±10 nm. We also did not observe the existence of any color halo similar to Newton's rings that might be associated with a variation in size of the rectangular cavity. Thus we conclude that the cavity was stable against thermal effects.

F. Pressure testing

The cavities were pressure tested to 6 bar when first cooled down. One cavity (for NMR) has been under measurement for more than 1 year with repeated cycles in pressure between vapor pressure and 6 bar. The second (circular cavity for the torsional oscillator) failed after multiple cool downs to helium temperatures at the junction point of the silver to silicon.

IV. SUMMARY

We have demonstrated the ability to fabricate, characterize, and reliably operate cavities a few hundred nanometer in thickness and having aspect ratios greater than 10 000. The cavities have no internal supports and can withstand pressures as high as 6 bar. The use of anodic bonding of glass to silicon allows us to optically characterize the cavities after assembly. Silicon-silver-epoxy joints also have been shown to survive multiple cool downs to cryogenic temperatures. New designs that span the parameter space from several μm down to the 100 nm scale are being planned to allow access to the nearly three-dimensional to quasi 2D limit in superfluid ^{3}He experiments.

ACKNOWLEDGMENTS

We acknowledge research funding support at Cornell from the NSF under Grant No. DMR-0457533, through the Cornell Materials Science Center under Grant No. DMR 0520404, and at Royal Holloway from the EPSRC under Grant Nos. EP/E054129/1 and EP/C522877/1. Fabrication was carried out at the Cornell Nano Fabrication Facility (CNF). We acknowledge useful discussions with Dr. Priya Sharma at Royal Holloway and the help of Dr. Andrew Fefferman with some of the figures.

[1] Y. Nagato and K. Nagai, Physica B **284**, 269 (2000).
[2] A. B. Vorontsov and J. A. Sauls, Phys. Rev. B **68**, 064508 (2003).
[3] A. B. Vorontsov and J. A. Sauls, Phys. Rev. Lett. **98**, 045301 (2007).
[4] A. J. Leggett, Rev. Mod. Phys. **47**, 331 (1975).
[5] A. Casey, J. Parpia, R. Schanen, B. Cowan, and J. Saunders, Phys. Rev. Lett. **92**, 255301 (2004).
[6] A. Córcoles, A. Casey, J. Parpia, R. Bowley, B. Cowan, and J. Saunders, AIP Conf. Proc. **850**, 99 (2006).
[7] S. G. Dimov, R. G. Bennett, B. Ilic, S. S. Verbridge, L. V. Levitin, A. D. Fefferman, A. Casey, J. Saunders, and J. M. Parpia, J. Low Temp. Phys. **158**, 155 (2010).
[8] Y.-H. Li and T.-L. Ho, Phys. Rev. B **38**, 2362 (1988).
[9] I. Rhee, F. M. Gasparini, A. Petrou, and D. J. Bishop, Rev. Sci. Instrum. **61**, 1528 (1990).
[10] G. Wallis and D. I. Pomerantz, J. Appl. Phys. **40**, 3946 (1969).
[11] T. R. Anthony, J. Appl. Phys. **54**, 2419 (1983).
[12] W.-P. Shih, C.-Y. Hui, and N. C. Tien, J. Appl. Phys. **95**, 2800 (2004).
[13] Hoya Corp., 101 Metro Drive, Suite 500, San Jose, CA 95110.
[14] *Machinery's Handbook*, 21st ed., edited by, E. Oberg, F. D. Jones, and H. L. Horton (Industrial, New York, 1980).
[15] J. J. Wortman and R. A. Evans, J. Appl. Phys. **36**, 153 (1965).
[16] R. G. Bennett, L. V. Levitin, A. Casey, B. Cowan, J. Parpia, and J. Saunders, J. Low Temp. Phys. **158**, 163 (2010).
[17] L.V. Levitin, R. G. Bennett, A. J. Casey, B. Cowan, J. Parpia, and J. Saunders, J. Low Temp. Phys. **158**, 159 (2010).
[18] L. V. Levitin, R. G. Bennett, A. Casey, B. P. Cowan, C. P. Lusher, J. Saunders, D. Drung, and Th. Schurig, Appl. Phys. Lett. **91**, 262507 (2007).
[19] J. D. Plummer, M. D. Deal, and P. B. Griffin, *Silicon VLSI Technology: Fundamentals, Practice and Modeling* (Prentice-Hall, New York, 2000), p. 319.
[20] Crystalbond 509, Structure Probe, Inc., 569 East Gay Street, West Chester, PA 19380, USA.
[21] Stycast 2850, Ellsworth Adhesives, W129 N10825 Washington Dr., Germantown, WI 53022, USA.
[22] W. Kern and D. A. Puotinen, RCA Rev. **31**, 187 (1970).
[23] E. Nazaretski, R. D. Merithew, R. O. Pohl, and J. M. Parpia, Phys. Rev. B **71**, 144201 (2005).